Many details relating to the formation of the microdomains and the structural modifications at the domain boundaries remain unknown and further studies on this interesting material are warranted, using high-resolution electron microscopy as well as inelastic neutron diffraction.

References

ALARIO-FRANCO, M. A., GREY, I. E., JOUBERT, J. C., VINCENT, H. & LABEAU, M. (1982). *Acta Cryst.* A**38**, 177–186.

BURSILL, L. A., NETHERWAY, D. J. & GREY, I. E. (1978). *Nature (London)*, **272**, 405–410.

CHEN, S., MORRIS, J. W. & KHACHATURYAN, A. G. (1979). *AIP Conf. Proc.* **53**, 168–172.

JEHANNO, G. (1965). PhD Thesis, Univ. of Paris.

KOVBA, L. M. & TRUNOV, V. K. (1962). *Dokl. Akad. Nauk SSSR*, **147**, 622–624.

LIPSON, H. (1972). *Optical Transforms*. London: Academic Press.

TRUNOV, V. K. & KOVBA, L. M. (1966). *Zh. Strukt. Khim.* **7**, 896–897.

Acta Cryst. (1982). A**38**, 761–772

Gaussian Growth-Disorder Models and Optical Transform Methods

BY T. R. WELBERRY AND C. E. CARROLL

Research School of Chemistry, Australian National University, PO Box 4, Canberra, ACT 2600, Australia

(*Received* 19 *January* 1982; *accepted* 6 *May* 1982)

Abstract

The properties of Gaussian growth-disorder models are explored and their use for producing realizations of disordered lattices for optical transform analogue experiments is described. Use of Gaussian variables provides greater flexibility than previously described binary ones and in particular enables realizations to be produced in dimensions greater than two without restriction on the values of nearest-neighbour correlation coefficients. A method of converting Gaussian realizations to binary ones is also described.

1. Introduction

Optical transform methods (Lipson, 1973) have become well established as aids in deducing the structure of materials from their X-ray diffraction patterns. Although for non-disordered single-crystal structure determination the method cannot compete with computer calculations, for non-crystalline or disordered materials the method still has considerable appeal, not least being the power of the visual presentation of results to stimulate thought and aid in the development of intuition. The production of an optical transform from a screen representing a complicated statistical distribution of atoms or molecules is just as readily performed as from one representing the simplest regular arrangement. With the advent of fast digital to film writing devices the production of the basic diffraction screen (Harburn, Miller & Welberry, 1974) is now readily performed under computer control.

However, while it is now possible to produce diffraction screens containing $\sim 10^6$ scattering points very rapidly and easily compared with the tedious manual techniques previously employed, the very size of the assembly presents quite a new problem. This concerns the way in which the actual distribution of scattering points is generated. The complicated statistical distribution of atoms and molecules mentioned above arises in nature in ways which must be mimicked in the generating computer program. While in principle the underlying physics may be understood sufficiently to make this possible, in practice the process is often far too lengthy for an assembly of points anywhere near as large as that desirable to obtain a good noise-free diffraction pattern, even for a simple physical model such as the spin-$\frac{1}{2}$ Ising model.

For this reason we have developed a number of stochastic models called 'growth-disorder models' (Welberry & Galbraith, 1973) which may be used to generate rapidly and easily, using a simple algorithm, spatial distributions of random variables having specific statistical properties. While these provide distributions less general than might be supposed to occur in real substances, they nevertheless still have considerable flexibility so that it is likely that any real physical effect may be approximated quite satisfactorily. Several examples in which these models have been used to

0567-7394/82/060761-12$01.00

assist in the interpretation of diffraction problems have already been reported (Welberry & Jones, 1980; Welberry, Miller & Carroll, 1981; Welberry, Jones & Epstein, 1982; Welberry, 1982).

To date the development of growth-disorder models has largely concentrated on the use of binary random variables with the intention that the two 'states' of the variables would represent, for example, alternative orientations of a molecule in a disordered molecular crystal, or two different atomic or molecular species in a solid solution. Certain classes of growth-disorder models are easily soluble (Welberry, 1977; Welberry, Miller & Pickard, 1979) and it is these models that have proved most useful for the generation of optical diffraction screens representing disordered lattice distributions.

Growth-disorder models have, however, some limitations which stem directly from the fact that they are 'grown' in a unilateral fashion from some predetermined boundary conditions. However, since it is this unilateral growth which allows the rapid generation of large arrays suitable for optical diffraction experiments, discarding this aspect in favour of say Ising-like models, which require lengthy iterative procedures to obtain realizations, is not generally feasible. One particular problem encountered in these models is that in three dimensions (3D) the range of statistical correlation values that can be built into lattice distributions is severely limited (see Welberry, Miller & Pickard, 1979) allowing only fairly small degrees of short-range order.

In order to extend the range of models available we have turned our attention to stochastic models which make use of continuous random variables, and in particular Gaussian variables. Initial investigations in the use of these variables suggested that some of the problems encountered with binary variables could be eliminated. In a recent paper we developed one aspect of these Gaussian models and we refer the reader to this paper for background references (Welberry, Miller & Carroll, 1980). In the present paper we develop Gaussian models in more detail and explain their use for a number of applications.

The structure of the paper is as follows. In § 2 we outline the theory of a 2D model on a rectangular lattice and place it in the context of more general models. In § 3 we derive the diffracted intensity distribution for a 2D model comprising two independent sets of random variables which represent atomic displacements in two orthogonal directions. Comparison is made with optical diffraction patterns. In § 4 we show how the same model may readily be extended to higher dimensions. In § 5 we describe a procedure to convert Gaussian realizations to binary ones. Finally, in § 6 we discuss from a practical view-point the use of Gaussian growth-disorder models for producing optical diffraction models of disordered lattices.

2. A two-dimensional model on a rectangular lattice

In an earlier paper (Welberry, Miller & Carroll, 1980) we considered the joint distribution of the four variables X_A,X_B,X_C,X_D on a single unit cell (see Fig. 1), namely

$$\begin{aligned}P(X_A,X_B,X_C,X_D) = K \exp\{-[&X_A^2 + X_B^2 + X_C^2 + X_D^2 \\ &- 2r(X_A X_B + X_C X_D) \\ &- 2s(X_A X_C + X_B X_D) \\ &+ 2rs(X_A X_D + X_B X_C)] \\ &\times [2\sigma^2(1-r^2)(1-s^2)]^{-1}\}. \quad (1)\end{aligned}$$

This distribution has rectangular symmetry (*mm*) and moreover will factorize as follows.

$$\begin{aligned}P(X_A,X_B,X_C,X_D) = P(X_A)\,P(X_B/X_A)\,P(X_C/X_A) \\ \times P(X_D/X_A,X_B,X_C), \quad (2)\end{aligned}$$

where

$$P(X_A) = K \exp\left\{\frac{-X_A^2}{2\sigma^2}\right\} \quad (3)$$

$$P(X_B/X_A) = K \exp\left\{\frac{-(X_B - rX_A)^2}{2\sigma^2(1-r^2)}\right\} \quad (4)$$

$$P(X_C/X_A) = K \exp\left\{\frac{-(X_C - sX_A)^2}{2\sigma^2(1-s^2)}\right\} \quad (5)$$

$$\begin{aligned}&P(X_D/X_A,X_B,X_C) \\ &= K \exp\left\{\frac{-(X_D - sX_B - rX_C + rsX_A)^2}{2\sigma^2(1-s^2)(1-r^2)}\right\}. \quad (6)\end{aligned}$$

The K's in the above equations (1)–(6) are normalization constants which are different in each expression. σ is the standard deviation of the random variable at a single site and r,s are nearest-neighbour correlation coefficients.

The above factorization allows us to construct, in a growth-disorder-model fashion, realization of lattice distributions in which the ensemble average of the distribution on the unit cell is given by (1). This is achieved by replacing the local site variables X_D,X_B,X_C,X_A by the lattice variables $X_{i,j}$, $X_{i-1,j}$, $X_{i,j-1}$, $X_{i-1,j-1}$ and using the conditional relations (2) to (6) successively to add points to the lattice. Such a construction is possible because the factorization, (2), implies the conditional independence relation that X_B is independent of X_C given X_A. [Note that the symmetry of (1) ensures that other symmetry-related conditions also hold.] This means that, in Fig. 1, when adding the point D using (6) we do not need simultaneously to consider the dependence of X_D on X_E and X_F. For further details of constructing lattice distributions see § 6.

In order to produce lattice realizations we simply use (3) for the first point, (4) and (5) for all points in

sequence along boundary edges and (6) for the remaining bulk of the lattice. In common with the corresponding binary model lattices (see Welberry, 1977; Pickard, 1980), lattices generated in this way are immediately stationary [*i.e.* $P(X_{i,j}, X_{i-1,j}, X_{i,j-1}, X_{i-1,j-1})$ is independent of i,j] and also have the property that Markov chains are embedded along every pathway in the lattice whose steps along each of the axes are always in the same direction. This implies that the correlations are geometric, *i.e.*

$$\rho_{kl} = r^{|k|} s^{|l|}, \tag{7}$$

where

$$\rho_{kl} = \frac{\langle X_{i-k} X_{j-l}\rangle - \langle X_i\rangle^2}{\langle X_i^2\rangle - \langle X_i\rangle^2}. \tag{8}$$

Here we use $\langle\ \rangle$ to denote expectation values over all i,j. For further details see Pickard (1980).

It is fruitful to consider an alternative treatment of such a lattice of Gaussian variables as that described above. We can consider the whole (say $n \times m$) lattice as a multivariate Gaussian distribution of $N\ (= n \times m)$ variables for which the probability density is given quite generally by

$$\frac{1}{(2\pi)^{N/2}(\det V)^{1/2}} \exp\left\{-\tfrac{1}{2}\sum_\alpha \sum_\beta X_\alpha (V^{-1})_{\alpha\beta} X_\beta\right\}, \tag{9}$$

where X_α is one of the zero mean variables and V is the $N \times N$ covariance matrix. V is a real symmetric matrix for which all the eigenvalues must be positive in order to have convergence of the Gaussian integral (see *e.g.* Rosenblatt, 1978, p. 28, or Miller, 1975, p. 7). A number of simplifications ensue if the N variables represent the variables on the $n \times m$ lattice and we require that we have translational symmetry (for finite n and m we wrap the lattice on a torus). In addition to providing that the variance of each variable is the same [*i.e.* $(V)_{\alpha\alpha} = \sigma^2$ for all α] the translational symmetry results in the matrix inversion becoming relatively simple.

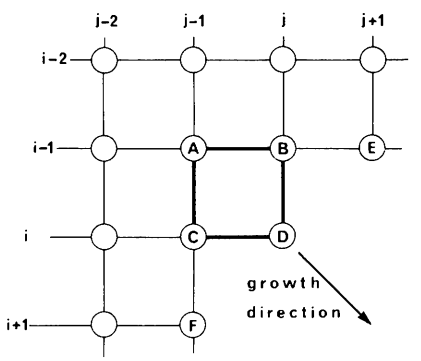

Fig. 1. Lattice-site labelling for the 2D growth-disorder model.

We make a further simplification of the general distribution (9) by requiring that the variables only interact with close neighbours, so that

$$\sum_\alpha \sum_\beta X_\alpha (V^{-1})_{\alpha\beta} X_\beta = \sum_i \sum_j X_{i,j}[AX_{i,j} + 2BX_{i-1,j} + 2CX_{i,j-1} + 2D(X_{i-1,j-1} + X_{i-1,j+1})], \tag{10}$$

i.e. each diagonal element of V^{-1} is A and off-diagonal elements are equal to B, C, D or zero.

The inversion of this simplified matrix to obtain the covariance matrix V can now be performed quite explicitly. In particular, this inversion gives the covariances associated with nearest-neighbour points in the axial and diagonal directions. If we define the variance, σ^2, and the nearest-neighbour correlation coefficients r,s by

$$\langle X_{i,j}{}^2\rangle = \sigma^2; \quad \langle X_{i,j-1} X_{i,j}\rangle = s\sigma^2; \quad \langle X_{i-1,j} X_{i,j}\rangle = r\sigma^2, \tag{11}$$

then the covariance matrices for the two variables associated with neighbouring sites of the lattice in the axial directions are

$$\sigma^2\begin{pmatrix} 1 & r \\ r & 1 \end{pmatrix} \quad \text{and} \quad \sigma^2\begin{pmatrix} 1 & s \\ s & 1 \end{pmatrix}.$$

The values of r and s may be obtained explicitly in terms of the interaction parameters A,B,C,D of (11). Similarly correlations between more distant neighbours may be determined, but in general these will not be simply related to the nearest-neighbour correlations r and s.

We now come to the crucial step which links this description to the growth-disorder model formulation described above. We find that by imposing one condition on A,B,C,D, namely

$$AD - BC = 0, \tag{12}$$

the covariance matrix takes on the simple form where correlations obey the geometric relation (8) and in particular the diagonal correlation, t say, is given by $t = rs$. We thus conclude that this special case of the general multivariate Gaussian distribution corresponds to the growth-disorder-model formulation expressed in (4)–(7). Further discussion of the cases $AD - BC \neq 0$ will be the subject of a future paper. For present purposes we confine our attention to the growth-disorder-model special case for which realizations are easily obtained *via* (4)–(7). We note in passing that this formulation in which the total multivariate distribution is obtained by multiplying together factors, which are themselves positive definite (for $r^2 < 1$, $s^2 < 1$), automatically ensures that the whole matrix V is also positive definite. The same result does not necessarily hold for cases other than (12) and it is necessary to

ensure that the whole matrix V is positive definite and not merely the sub-matrices referring to nearest neighbours.

3. Diffracted intensity distribution from a simple two-dimensional model

It is instructive to consider a particular example of a 2D Gaussian growth-disorder model in order to obtain some feeling for the general properties which might carry over to more complicated models, and to provide illustrations which can be compared to theory. For this purpose we choose to discuss a 2D model on a square lattice with one atom per unit cell in which displacements of the atoms from their mean positions are specified by two sets of random variables $X_{l,m}$ and $Y_{l,m}$. Here we have changed the indices specifying the lattice for convenience, and for the same reason we assume the lattice constants to be unity. Hence the atom position corresponding to the (l,m)th lattice point is

$$x = l + X_{l,m}$$
$$y = m + Y_{l,m}.$$

In general, the zero-mean Gaussian random variables $X_{l,m}$ and $Y_{l,m}$ may be correlated. That is to say that the principal directions of the displacement tensor are not parallel to the axes x and y. We can define a new pair of sets of random variables $X'_{l,m}$ and $Y'_{l,m}$ where

$$X'_{l,m} = X_{l,m}\cos\theta + Y_{l,m}\sin\theta \qquad (13a)$$
$$Y'_{l,m} = -X_{l,m}\sin\theta + Y_{l,m}\cos\theta \qquad (13b)$$

which are uncorrelated. That is to say

$$\langle X'^2_{l,m}\rangle = A; \quad \langle Y'^2_{l,m}\rangle = B; \quad \langle X'_{l,m}\,Y'_{l,m}\rangle = 0. \qquad (14)$$

We then assume that each set of random variables $X'_{l,m}$ and $Y'_{l,m}$ is obtained *via* a growth-disorder-model construction so that ensemble averages of the lattice distributions may be expressed in terms of the original $X_{l,m}$ and $Y_{l,m}$. Because of translational invariance we need only consider

$$\langle X_{l,m}\,X_{0,0}\rangle = A\cos^2\theta\, r^{|l|}\,s^{|m|} + B\sin^2\theta\, t^{|l|}\,u^{|m|} \qquad (15)$$

$$\langle X_{l,m}\,Y_{0,0}\rangle = \langle Y_{l,m}\,X_{0,0}\rangle = A\sin\theta\cos\theta\, r^{|l|}\,s^{|m|} - B\sin\theta\cos\theta\, t^{|l|}\,u^{|m|} \qquad (16)$$

and

$$\langle Y_{l,m}\,Y_{0,0}\rangle = A\sin^2\theta\, r^{|l|}\,s^{|m|} + B\cos^2\theta\, t^{|l|}\,u^{|m|}. \qquad (17)$$

The four nearest-neighbour correlation coefficients r, s, t and u refer to the following interactions: r is the correlation between neighbouring X' displacements in the x direction; s is the correlation between neighbouring X' displacements in the y direction; t is the correlation between neighbouring Y' displacements in the x direction; u is the correlation between neighbouring Y' displacements in the y direction. Note that cross correlations, between for example the X' displacement of one atom with the Y' displacement of its neighbour, are zero.

Neglecting constant factors such as atomic scattering factors we can write the scattered intensity from such a model as

$$I = \sum_{l_1}\sum_{l_2}\sum_{m_1}\sum_{m_2}\exp\left[ik_x(l_1 - l_2 + X_{l_1,m_1} - X_{l_2,m_2}) + ik_y(m_1 - m_2 + Y_{l_1,m_1} - Y_{l_2,m_2})\right]. \qquad (18)$$

If we wrap the lattice around a torus, the model has translational symmetry, and we may write the average intensity as

$$I = \sum_l\sum_m \exp(ik_x l + ik_y m)\,\langle\exp\left[ik_x(X_{l,m} - X_{0,0}) + ik_y(Y_{l,m} - Y_{0,0})\right]\rangle. \qquad (19)$$

Substituting for the averages of the Gaussians from (15), (16) and (17) the intensity expression becomes the sum of two terms; a Bragg intensity and a diffuse intensity.

$$I(\mathbf{k})_{\text{Bragg}} = \exp(-2W)\sum_l\sum_m \exp(ik_x l + ik_y m) \qquad (20)$$

$$I(\mathbf{k})_{\text{diffuse}} = \exp(-2W)\sum_l\sum_m \{\exp[2W_A\, r^{|l|}\,s^{|m|} + 2W_B\, t^{|l|}\,u^{|m|}] - 1\} \times \exp(ik_x l + ik_y m). \qquad (21)$$

Using a power-series expansion for the exponential and then using the binomial theorem, we obtain

$$I(\mathbf{k})_{\text{diffuse}} = \exp(-2W)\sum_P\sum_Q \frac{(2W_A)^P(2W_B)^Q}{P!\,Q!} \times \left[\frac{1 - r^{2P}\,t^{2Q}}{1 + r^{2P}\,t^{2Q} - 2r^P\,t^Q\cos(k_x)}\right] \times \left[\frac{1 - s^{2P}\,u^{2Q}}{1 + s^{2P}\,u^{2Q} - 2s^P\,u^Q\cos(k_y)}\right]. \qquad (22)$$

Here P and Q are non-negative integers and $P = Q = 0$ is excluded from the sum. The term $\exp(-2W)$ is the 'Debye–Waller' factor with

$$2W = 2W_A + 2W_B = A(k_x\cos\theta + k_y\sin\theta)^2 + B(-k_x\sin\theta + k_y\cos\theta)^2. \qquad (23)$$

It may be shown that the sum over P and Q always converges but the convergence is slow if $2W_A$ or $2W_B$ or both are large quantities. For small W_A and W_B and $r,s,t,u \ll 1$ only the leading terms of (22) need be

considered. Each of these is seen to be a set of fringes with a profile given by the familiar diffuse-peak formula as given, for example, by Guinier (1963), p. 269. Each set of diffuse fringes is modified by a factor stemming from the $W_A^P\ W_B^Q/P!Q!$ term in (22) which has a node or zero line passing through the origin of reciprocal space and lying normal to the direction of displacement of the independent random variable X' or Y' from which the set of fringes originates. The fact that even for small values of the mean-square amplitudes A and B the values of W_A and W_B become appreciable at large angles in reciprocal space means that at high angles more terms of (23) must be included. This has the effect of broadening the diffuse fringes stemming from the primary correlation. We illustrate these effects by showing some examples of optical transforms of the model in Fig. 2.

In all cases in Fig. 2 the X' variables represent displacements in a direction approximately 30° above horizontal to the left, and the Y' variables represent displacements normal to these approximately 30° from the vertical. In Fig. 2(*a*) the X' variables have a standard deviation of 5% of the lattice spacing and are correlated with coefficients of 0·7 vertically and 0·3 horizontally. The Y' variables have zero amplitude. In Fig. 2(*b*) the X' variables have zero amplitude and the Y' variables a 5% standard deviation with correlations of −0·7 vertically and −0·3 horizontally. Fig. 2(*c*) has the same X' values as in Fig. 2(*a*) but now the Y' variables also have a 5% standard deviation but are uncorrelated. Similarly, Fig. 2(*d*) has the same Y' values as in Fig. 2(*b*) but the X' variables now also have a 5% deviation but are uncorrelated. Fig. 2(*e*) shows both X' and Y' variables together with 5% standard deviations and the same correlation values of 0·7 and 0·3 for X' and −0·7 and −0·3 for Y'. Finally, in Fig. 2(*f*) these same correlation values are present but the standard deviation of the X' variables has been increased to 15%.

4. Extension to higher dimension

Both the joint distribution on the unit cell, (1), and the corresponding conditional probability factors, (3) to (6), are easily carried over into 3D and higher dimensions. Expressions may be written down by inspection but at least for the 3D case the conditional probability factors have been combined and the form of the joint distribution verified.

Consider the 3D unit cell *ABCDEFGH* in Fig. 3. In an analogous way to (2) we require the general joint distribution on the unit cell to factorize in the following way.

$$\begin{aligned} P[X_A,X_B,X_C,X_D,X_E,X_F,X_G,X_H) &= P(X_A)\,P(X_B/X_A) \\ &\times P(X_C/X_A)\,P(X_E/X_A)\,P(X_D/X_A,X_B,X_C) \\ &\times P(X_F/X_A,X_B,X_E)\,P(X_G/X_A,X_C,X_E) \\ &\times P(X_H/X_A,X_B,X_C,X_D,X_E,X_F,X_G). \end{aligned} \tag{24}$$

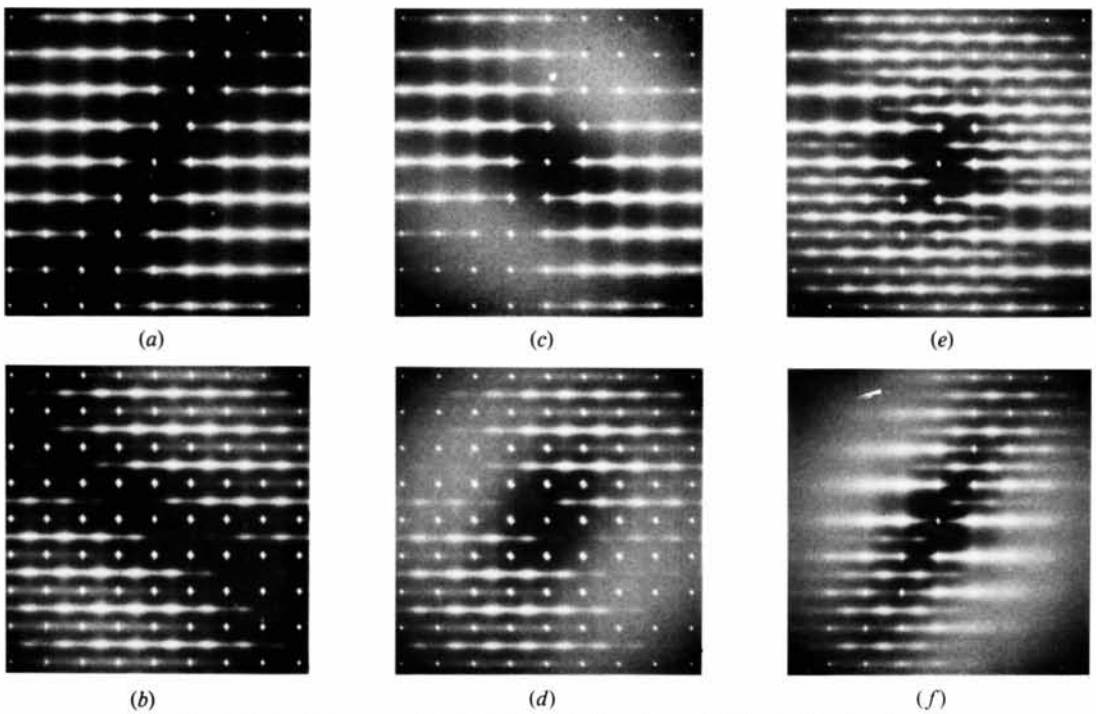

Fig. 2. Optical transforms for the 2D growth-disorder model. See text for details.

The conditional probabilities which refer to the 2D faces of the cell have a form given by (6) with the two correlations appropriate for that face, while the final term in (24) may be written

$$P(X_H/X_A,X_B,X_C,X_D,X_E,X_F,X_G) = K \exp\{[-(X_H - rX_G - sX_F - tX_D + rtX_C + stX_B + rsX_E - rstX_A)^2] \times [2\sigma^2(1-s^2)(1-r_2)(1-t^2)]^{-1}\} \quad (25)$$

In four dimensions the distribution on the 16 points of the hypercubic cell depicted in Fig. 3 may be split into conditional probability factors which refer to four 3D volumes, six 2D faces and four 1D edges, along which the primary correlations r, s, t and u run. By analogy with (25) the form of the final term involving the probability of P given the fifteen other points on the hypercube is

$$P(X_P/X_A,\ldots,X_O) = K \exp\{-(X_P - rX_O - sX_N - tX_L - uX_H + suX_F + stX_J + tuX_D + ruX_G + rsX_M + rtX_K - rstX_I - rsuX_E - rutX_C - sutX_B + rstuX_A)^2 \times [2\sigma^2(1-r^2)(1-s^2)(1-t^2)(1-u^2)]^{-1}]\}. \quad (26)$$

The property of the geometric correlation field is carried over into these higher dimensions.

Our prime concern in formulating these higher-dimensional models has been to facilitate the computer generation of optical diffraction masks to model disorder problems encountered in X-ray diffraction. However, while these distributions are necessarily two dimensional, the employment of projections of higher-dimensional models adds considerable diversity to the distributions that may be achieved and examples of these are given in § 6.

5. Conversion of Gaussian to binary models

Many problems of disorder that arise in X-ray diffraction can appropriately be described in terms of binary variables, *e.g.* the substitutional disorder in molecular crystals (see *e.g.* Welberry & Jones, 1980). It was for this reason that our early interest in growth-disorder models concentrated on binary models. However, although useful 2D binary models were developed (Welberry, 1977) the extension to 3D (Welberry, Miller & Pickard, 1979) proved exceedingly tedious and moreover provided only a restricted range of short-range-order properties. For this reason we investigate the possibility of converting the present Gaussian growth-disorder models to binary ones since they are easily formulated in higher dimensions and also provide a complete range of nearest-neighbour correlation values.

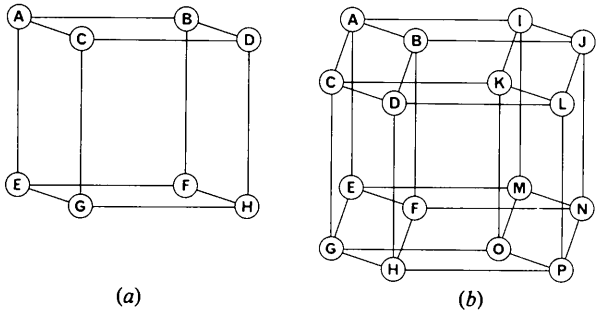

(*a*) (*b*)

Fig. 3. Site labelling for (*a*) 3D and (*b*) 4D growth-disorder model.

The aim therefore is as follows. We use a Gaussian model to produce realizations of a disordered lattice. Each Gaussian random variable, $X_{i,j}$ say, is then converted to a binary variable, $Y_{i,j}$ say, by setting

$$\left.\begin{aligned} Y_{i,j} &= -1 \quad \text{for } X_{i,j} < c \\ Y_{i,j} &= +1 \quad \text{for } X_{i,j} > c \end{aligned}\right\}. \quad (27)$$

We seek to find the relationship between the binary concentration, $\theta = (1 + \langle Y_{i,j}\rangle)/2$ and the constant c, and more importantly the relationship between correlation coefficients r_g between two Gaussian variables and r_b between the corresponding binary variables.

We first consider the simple case when $c = 0$ and θ is evidently 0·5. The Gaussian probability density for two real variables which have zero mean and unit variance is

$$P(x,y) = \frac{1}{2\pi(1-r^2)^{1/2}} \exp\left[-\frac{x^2+y^2}{2(1-r_g^2)} + \frac{r_g xy}{(1-r_g^2)}\right] \quad (28)$$

The correlation coefficient between the resulting binary variables is

$$r_b = \frac{1}{2\pi(1-r_g^2)^{1/2}} \times \int_{-\infty}^{\infty}\int_{-\infty}^{\infty} \operatorname{sign}(x)\operatorname{sign}(y) \times \exp\left[-\frac{x^2+y^2}{2(1-r_g^2)} + \frac{r_g xy}{(1-r_g^2)}\right] dx\,dy. \quad (29)$$

Putting $p = xy$ and $q = x/y$ and treating the four quadrants separately we find

$$r_b = \frac{1}{\pi(1-r_g^2)^{1/2}} \left\{ \int_0^{\infty}\int_0^{\infty} \exp\left[\frac{-p(q+q^{-1}-2r_g)}{2(1-r_g^2)}\right] \frac{dp\,dq}{2q} - \int_0^{\infty}\int_0^{\infty} \exp\left[\frac{-p(q+q^{-1}+2r_g)}{2(1-r_g^2)}\right] \frac{dp\,dq}{2q} \right\}$$

Integrating over p and then over q gives

$$r_b = \frac{2}{\pi} \arcsin(r_g). \quad (30)$$

From this result we first note that r_b can take values over the whole range from -1 to $+1$. In addition, we

see that, except for the three points $r_g = r_b = -1, 0, +1$, $|r_b| < |r_g|$. This second property affects the way in which correlations decay with distance and we will no longer have the geometric form characteristic of simple binary or Gaussian growth-disorder models.

It is interesting to compare the way in which the low-order correlations decay. In Table 1 we list values of the first four correlation values for three models: (*a*) a Gaussian or simple binary model with a first-order correlation of 0·6366; (*b*) a rectified Gaussian model from this work with a binary correlation value of 0·6366; (*c*) the two-dimensional Ising model on a square lattice, at the transition temperature, in the [11] direction (see Cheng & Wu, 1967). It is seen from Table 1 that in respect of the way correlations decay with distance, the rectified Gaussian model is a better approximation to the Ising model than the simple Gaussian or binary growth-disorder models themselves.

We next consider the more difficult case of $c \neq 0$. Referring again to the bivariate Gaussian probability density, (28), we find the binary concentration, θ, by considering

$$\langle \text{sign}\,(x-c)\rangle = 2\theta - 1 = -\text{erf}\,(2^{-1/2}\,c). \quad (31)$$

To obtain c we use Newton's rule and an approximate computation of $\text{erf}(2^{-1/2}\,c)$ (Hastings, 1957, p. 169). For the binary correlation, r_b, we consider

$$\begin{aligned} P_{\text{av}} &= \langle \text{sign}\,(x-c)\,\text{sign}\,(y-c)\rangle \\ &= r_b + (1-r_b)\,[\text{erf}\,(2^{-1/2}\,c)]^2. \end{aligned} \quad (32)$$

we proceed as follows:

$$P_{\text{av}} = \int_{\infty}^{\infty}\int_{\infty}^{\infty} \frac{\text{sign}\,(x-c)\,\text{sign}\,(y-c)}{2\pi(1-r_g^2)^{1/2}} \times \exp\left[-\frac{x^2+y^2-2r_g\,xy}{2(1-r_g^2)}\right] dx\,dy.$$

Putting the sign function in the integral form $\text{sign}\,(x) = (1/\pi)\int_{-\infty}^{\infty} (\sin \alpha x)/\alpha\, d\alpha$ and using the Fourier transform of the Gaussian probability density, we obtain after some algebra

$$\frac{dP_{\text{av}}}{dr_g} = \left(\frac{2}{\pi}\right)(1-r_g^2)^{-1/2} \exp\left(-\frac{c^2}{1+r_g}\right).$$

Table 1. *Comparison of the low-order correlation coefficients of growth-disorder models with those for the Ising model at the transition temperature*

	First	Second	Third	Fourth
Simple binary	0·6366	0·4053	0·2580	0·1643
Rectified Gaussian	0·6366	0·5008	0·4063	0·3343
Ising [11] direction	0·6366	0·5404	0·4893	0·4556

Hence

$$\frac{\pi}{4}(1-P_{\text{av}})\exp\left(\frac{c^2}{2}\right) = \int_0^R \frac{1}{(x^2+1)} \exp\left(-\tfrac{1}{2}c^2\,x^2\right) dx. \quad (33)$$

Here R is related to the Gaussian correlation, r_g, by

$$R = \left(\frac{1-r_g}{1+r_g}\right)^{1/2}. \quad (34)$$

Thus for given values of P_{av} and c we need to solve (33) for R and hence obtain r_g, the Gaussian correlation required to produce the desired binary correlation r_b. To do this we use a numerical technique based on Newton's rule. From (33) we find successive approximations.

$$\begin{aligned} R_{n+1} = R_n &+ (1+R_n^2)\exp\left(\frac{c^2 R_n^2}{2}\right) \\ &\times \left[\frac{\pi}{4}(1-P_{\text{av}})\exp\left(\frac{c^2}{2}\right) - \int_0^{R_n} \frac{1}{x^2+1}\exp\left(\frac{-c^2x^2}{2}\right)dx\right]. \end{aligned} \quad (35)$$

For the first approximation, R_1, we use the following form which gives the correct value for R in three cases; $R = 0$, $R = 1$, $R \to \infty$.

$$\begin{aligned} R_1 = (1-P_{\text{av}})\{&(1+\text{erf}(2^{-1/2}|c|)) \\ &\times [P_{\text{av}} + 1 - 2\,\text{erf}(2^{-1/2}|c|)]^{1/2}\}^{-1}. \end{aligned} \quad (36)$$

In practice we have found satisfactory convergence for the above procedure except in cases involving large negative correlations, although our investigations have mainly been confined to regions where $0{\cdot}3 < \theta < 0{\cdot}7$.

6. The use of Gaussian growth-disorder models for producing optical diffraction models of disordered lattices

In this section we discuss examples designed to illustrate the use of Gaussian growth-disorder models in optical transform work, but first we discuss briefly the practical details of how realizations are produced and optical transforms made.

For all examples the actual Gaussian model is used in the conditional probability form typified by (3)–(6). These are univariate Gaussian distributions and as such are directly amenable to use in a computer program in conjunction with a pseudo-random-number generator. Particular care must be taken with regard to the latter since standard generators often contain unwanted correlations. Our procedure is as follows. Uniformly distributed pseudo-random numbers are first obtained

from the Fortran library routine *RANDU* on our Digital Equipment PDP-11. To improve the randomness of these numbers a buffer of 100 values is stored in memory. For each number used two calls to *RANDU* are required. The first is used to select at random one value from the buffer and the second replaces the extracted value with a new one. To generate Gaussian distributed random numbers from these we currently use the polar method of Marsaglia described in James (1980).

Realizations of lattice distributions are written directly onto film using an Optronics P-1700 Photomation System (see Harburn, Miller & Welberry, 1974). Optical diffraction patterns are recorded using a laser diffractometer similar to that described by Harburn, Taylor & Welberry (1975). The films are frequently used directly in air, which introduces some phase errors in the Fourier transform due to variations in film and emulsion thickness. For most purposes involving the short-range effects in which we are interested and for the fine scale of plot that we employ the errors are not serious and present themselves only as a flare around Bragg peaks. Enclosing the film in an optical gate containing a medium whose refractive index is matched to that of the film can largely remove these errors, but is much more tedious to use.

In the first example we illustrate the use of Gaussian variables to represent rigid-body motion in a molecular crystal. We describe a hypothetical structure of benzene with molecules placed at the nodes of a square lattice. The Gaussian random variables are used to represent either displacements (horizontally and vertically) or librations about an axis in the plane of the paper. Correlations between neighbouring molecular displacements or orientations are introduced to model the effect of acoustic phonons. Fig. 4(*a*) shows a small portion of a typical diffraction screen; the originals contained ~30000 molecules. Figs. 4(*b*)–(*f*) show optical transforms of screens in which various effects have been included. For Fig. 4(*b*) each molecule was allowed independently to be displaced by a Gaussian variable from its mean position in each of two independent directions. On a scale where the side of the hexagon is 1·4 Å the standard deviation is 0·122 Å. For Fig. 4(*c*) each molecule was allowed independently to be rotated about the centre of mass by an amount given by a single Gaussian variable with a standard deviation of 5°. For Fig. 4(*d*) the same distribution for a single molecule as in Fig. 4(*c*) was included but neighbouring molecular orientations were now correlated with coefficients of 0·5 in both directions. For Fig. 4(*e*) the same distribution for a single molecule as in Fig. 4(*b*) was included but neighbouring molecular displacements were now correlated with coefficients of 0·5, both transverse and longitudinal in both directions. Finally, in Fig. 4(*f*) both translations and displacements were included (independently) and again all nearest-neighbour correlation coefficients were 0·5.

We now discuss an example designed to illustrate the use of multidimensional growth-disorder models. While the realizations which are used for optical diffraction are necessarily two dimensional the problems encoun-

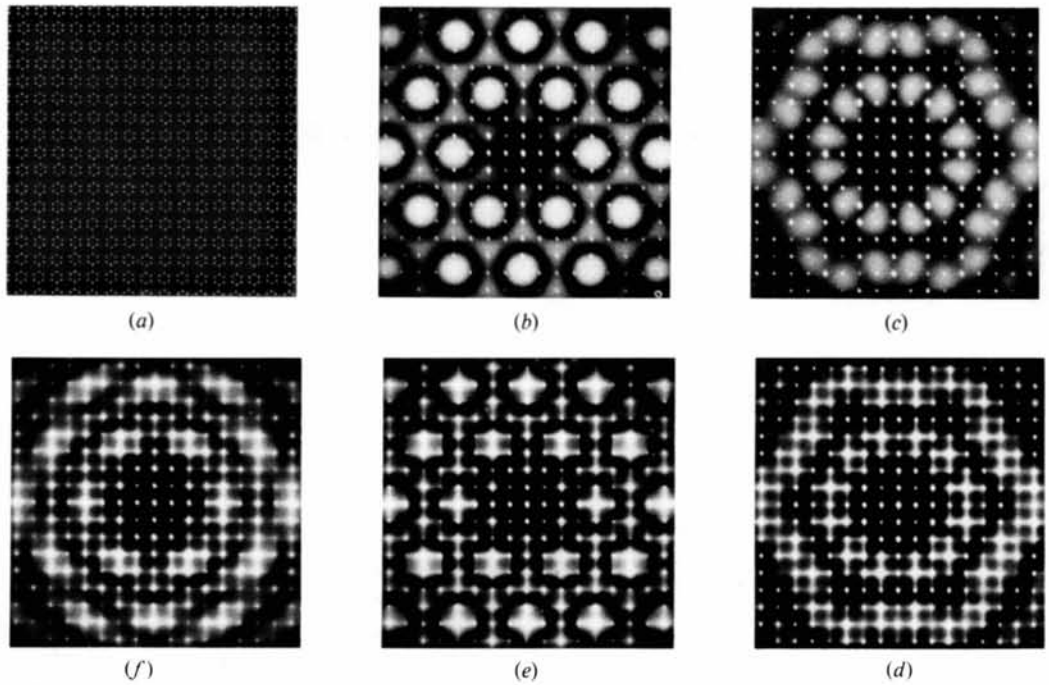

Fig. 4. A small representative portion of a typical diffraction mask and optical transforms showing the use of Gaussian growth-disorder models for thermal perturbations in molecular crystals. See text for details.

tered in X-ray diffraction are often fully three-dimensional, and we need to consider a projection of such distributions. Furthermore, since it is realized that a growth-disorder model cannot produce the most general distribution on a given lattice, additional flexibility can often be obtained by using projections onto two dimensions of higher-dimensional models. In the example we discuss here we show how the same 2D structure can be considered as a projection from 3D or 4D in addition to the more obvious 2D representation and we explore the resulting diversification of the derived diffraction patterns.

In addition we use the Gaussian-to-binary conversion procedure so that in the illustrated realizations the short-range order is more readily apparent. However, for convenience we shall refer to the Gaussian correlation coefficients, r_g, that were used, rather than the resulting binary correlations, r_b. The 'concentration' in all cases was 0·5 so (30) should be used for the conversion.

Fig. 5 illustrates the example. We have a square lattice which has four atomic positions per unit cell and we suppose that each of the four positions is either occupied (dot) or unoccupied (black). The four positions within one unit cell are in the form of a square sub-unit which is rotated by about 18° to the axial directions of the lattice. Three different ways in which these sites may be linked to neighbours are shown and growth-disorder models may be used to introduce correlations along these 'bonds'. In each of the three figures four distinct primary correlations may be introduced. These are shown by the four heavy lines and in all cases each of the remaining vectors is identical to that one of these primary vectors to which it is parallel.

The connections or linkages for Fig. 5(*c*) correspond to the 4D model discussed in § 4 and the growth-disorder model construction for this topology uses the factorization of the 16-point distribution on (A, B, ..., P) discussed above, (26). Vectors such as AI, BJ, CG and AE correspond to cell repeats in the 2D realization while the other two dimensions are used to relate positions within the unit cell by vectors such as AB and AC. The connections shown in Figs. 5(*a*) and (*b*) correspond to alternative factorizations of the same 16-point distribution. Fig. 5(*a*) corresponds to a factorization in which only conditional probabilities relating to 2D growth-disorder models are involved, while Fig. 5(*b*) corresponds to a factorization involving 3D terms. Thus, for example, Fig. 5(*b*) corresponds to the factorization

$$\begin{aligned}P(X_A,\ldots,X_P) = {} & P(X_A)\,P(X_B/X_A)\,P(X_C/X_A)\\ & \times P(X_D/X_A,X_B,X_C)\\ & \times P(X_I/X_A)\;P(X_K/X_A,X_C,X_I)\\ & \times P(X_J/X_A,X_B,X_I)\\ & \times P(X_L/X_A,X_B,X_C,X_D,X_I,X_J,X_K)\\ & \times P(X_E/X_C)\,P(X_F/X_C,X_D,X_E)\\ & \times P(X_M/X_E,X_C,X_K)\\ & \times P(X_N/X_C,X_D,X_E,X_F,X_K,X_L,X_M)\\ & \times P(X_G/X_E)\,P(X_H/X_G,X_E,X_F)\\ & \times P(X_O/X_E,X_G,X_M)\\ & \times P(X_P/X_E,X_F,X_G,X_H,X_M,X_N,X_O).\end{aligned}$$

It is not feasible here to explore the full four-dimensional correlation space for each of these examples and in Figs. 6 and 7 we compare only a selection of realizations and their transforms. The samples of the realizations shown in Fig. 6 are small sections of those used to obtain the transforms shown in Fig. 7. The original diffraction masks contained about 10^5 unit cells or 2×10^5 scattering points. The vertical columns of examples shown have constant values of the 'internal' correlations r_{AB} and r_{AC}. The left column has $r_{AB} = r_{AC} = -0{\cdot}8$; the central column $r_{AB} = r_{AC} = 0{\cdot}0$; and the right column, $r_{AB} = r_{AC} = +0{\cdot}8$. The four rows of examples explore the effect of the different topologies by showing the patterns when each of the primary correlations r_{CE}, r_{BI} for 2D, r_{CE}, r_{AI} for 3D and r_{AE}, r_{AI} for 4D takes a value of $-0{\cdot}4$ (rows 2, 3 and 4). The top row shows the patterns when all but the 'internal' correlations. r_{AB} and r_{AC}, are zero. The relationship of

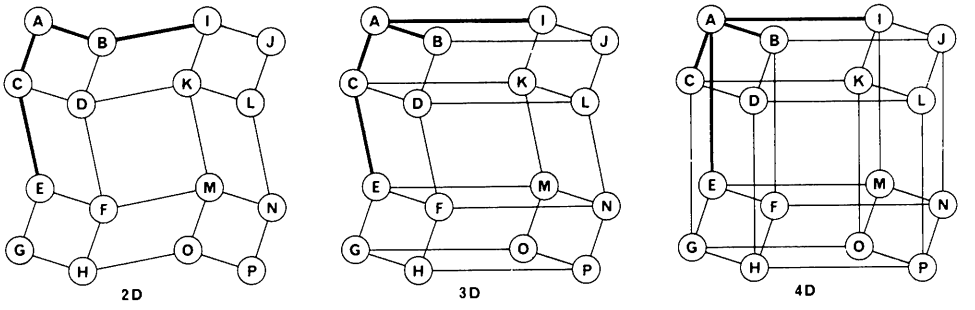

(*a*) (*b*) (*c*)

Fig. 5. Different ways in which the same 2D arrangement of atomic sites can be linked using different-dimension growth-disorder models.

the realizations to Fig. 5 is most apparent when the internal correlations are positive and square sub-units occur fully occupied quite frequently, as for example in Fig. 6(*c*).

The difference between the three topologies is most evident in the central column where the 'internal' correlations are zero. In Fig. 7(*e*) the transform shows diffuse fringes normal to and of a spacing reciprocal to the vectors *BI* and *CE*, with a minimum passing through the origin because of the negative correlation. In Fig 7(*h*) there are still the same fringes normal to *CE*, but in the horizontal direction the fringing is due to

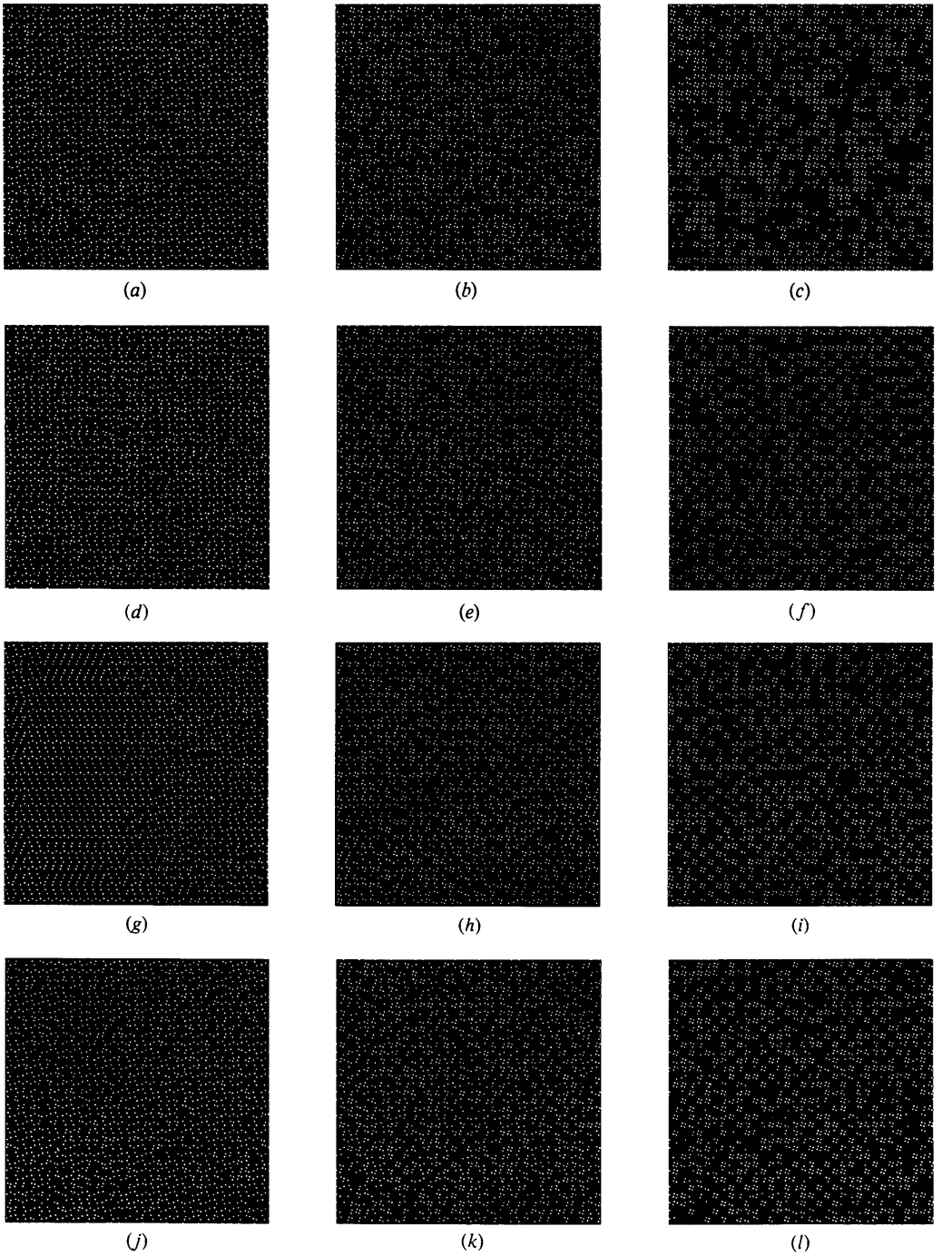

Fig. 6. Examples of diffraction screens for the models shown in Fig. 5. See text for details.

the longer cell vector AI. In Fig. 7(k) the fringes are normal to the longer vectors in both directions and the diffuse pattern shows the full symmetry of the square unit cell.

The effect of the 'internal' correlations r_{AB} and r_{AC} is evident in the top row of photographs where the diffuse fringes show clearly the 18° rotation of the square sub-units. For all examples in each of the columns the broad features of the distribution of intensity follows that seen most clearly in the top row, but this overall distribution is modified by the between-cell correlations. Here interesting differences arise because of the different topologies. Let us compare the 2D and 3D examples for the negative 'internal' correlations, Figs.

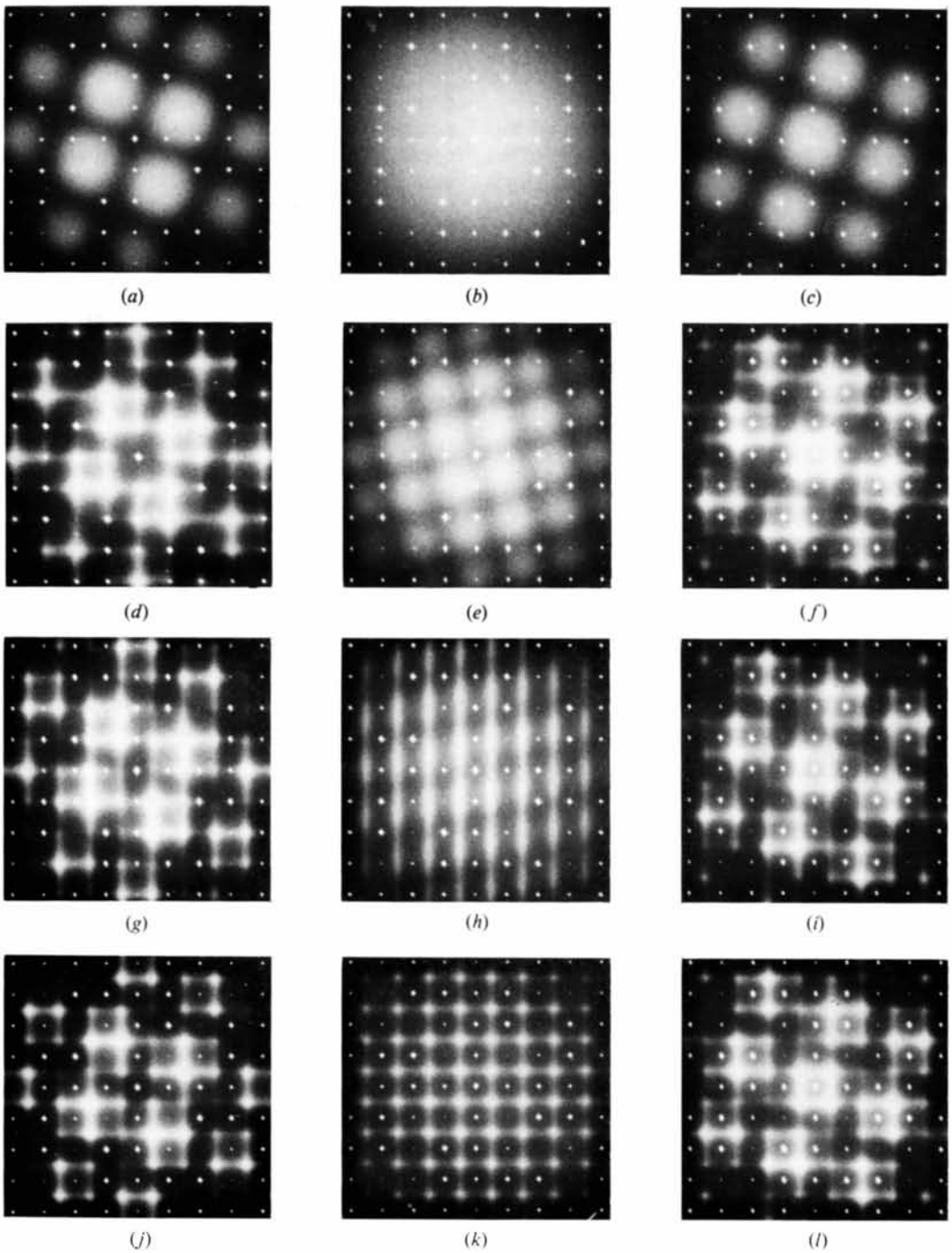

Fig. 7. Optical transforms corresponding to lattice realizations, small portions of which appear in Fig. 6.

7(*d*) and (*g*). For the 2D case, since r_{AB} and r_{BI} are both negative the correlation for the cell repeat, r_{AI}, is positive and the fringes in Fig. 7(*d*) are seen to coincide with rows of Bragg peaks. In the 3D case of Fig. 7(*g*), r_{AI} is set to be negative and hence the fringes occur between the vertical rows of Bragg peaks. For the corresponding examples with positive 'internal' correlation, Figs. 7(*f*) and (*i*), the difference is less marked since in this case the vector *AI* has a negative correlation in both cases. For the 3D case it is −0·4 by definition while for the 2D case it is the product of r_{AB} = +0·8 and r_{BI} = −0·4. The fringes for the 2D case are seen to be somewhat more diffuse.

The three different topologies illustrated in this example are by no means the only factorizations of the basic 16-point distribution that it is possible to use for a growth-disorder model procedure. Nevertheless they serve to illustrate that suitable choice of the factorization allows considerable diversity in the way in which interactions can be built into lattices with the use of growth-disorder models. The diversity is such that for use in tackling problems in X-ray diffraction it is likely that a distribution approximating that desired can be found by this means.

7. Conclusion

The three main developments that have stemmed from the current work are:

(i) the ability to represent disorder problems in which a description in terms of a continuous Gaussian variable is appropriate, *e.g.* thermal perturbations;

(ii) the ability to produce realizations in 3D or higher dimensions with no restriction on the range of nearest-neighbour correlations;

(iii) the ability to work entirely with Gaussian variables and to convert these to binary variables where appropriate.

Together these three properties represent a considerable increase in the flexibility of growth-disorder models for producing disordered lattice realizations suitable for optical analogue modelling of problems encountered in X-ray diffraction experiments.

There are two aspects of growth-disorder models which remain somewhat unsatisfactory, however. The first of these is that construction of the lattice must always use the square as the basic unit in 2D (or the cube in 3D). The growth-disorder-model solutions, of the type described here, impose the condition that correlations along the diagonals of such units must be the product of correlations along the edges. If we consider the triangle (or the tetrahedron in 3D) to be the more natural basic unit this means that correlations along the three edges cannot be chosen independently but must conform to the 'product rule' that the correlation along one side is the product of the correlations along the other two. The second, though related, aspect is that the resulting correlation field is decidedly non-isotropic since the correlation coefficients given by equations such as (7) necessarily imply that the correlations along the axes decay more slowly than in the diagonal directions. The result of this is that diffuse diffraction peaks have a decided 'cross-shape' appearance rather than the more rounded appearance that more general distributions might yield. Future work will be aimed at further exploration of these aspects of growth-disorder models.

References

CHENG, H. & WU, T. T. (1967). *Phys. Rev.* **164**, 719–735.

GUINIER, A. (1963). *X-ray Diffraction*. San Francisco: Freeman.

HARBURN, G., MILLER, J. S. & WELBERRY, T. R. (1974). *J. Appl. Cryst.* **7**, 36–38.

HARBURN, G., TAYLOR, C. A. & WELBERRY, T. R. (1975). *Atlas of Optical Transforms*. London: Bell.

HASTINGS, C. (1957). *Approximations for Digital Computers*. Princeton Univ. Press.

JAMES, F. (1980). *Rep. Prog. Phys.* **43**, 1145–1189.

LIPSON, H. (1973). *Optical Transforms*. New York: Academic Press.

MILLER, K. S. (1975). *Multivariate Distributions*. New York: Krieger.

PICKARD, D. K. (1980). *Adv. Appl. Probab.* **12**, 655–671.

ROSENBLATT, M. (1978). *Studies in Mathematics*, Vol. 18. *Studies in Probability Theory*. Washington: Mathematical Association of America.

WELBERRY, T. R. (1977). *Proc. R. Soc. London Ser. A*, **353**, 363–376.

WELBERRY, T. R. (1982). *Acta Cryst.* B**38**, 1921–1927.

WELBERRY, T. R. & GALBRAITH, R. (1973). *J. Appl. Cryst.* **6**, 87–96.

WELBERRY, T. R. & JONES, R. D. G. (1980). *J. Appl. Cryst.* **13**, 244–251.

WELBERRY, T. R., JONES, R. D. G. & EPSTEIN, J. (1982). *Acta Cryst.* B**38**, 1518–1525.

WELBERRY, T. R., MILLER, G. H. & CARROLL, C. E. (1980). *Acta Cryst.* A**36**, 921–929.

WELBERRY, T. R., MILLER, G. H. & PICKARD, D. K. (1979). *Proc. R. Soc. London Ser. A*, **367**, 175–192.